A multiphysics model of large-scale compact PV–CSP hybrid plants

Dounia Ziyati, Alain Dollet, Gilles Flamant, Yann Volut, Emmanuel Guillot, Alexis Vossier

A multiphysics model of large-scale compact PV–CSP hybrid plants

Dounia Ziyati, Alain Dollet, Gilles Flamant, Yann Volut, Emmanuel Guillot, Alexis Vossier

A multiphysics model of large-scale compact PV-CSP hybrid plants

Dounia Ziyati[a], Alain Dollet[a], Gilles Flamant[a], Yann Volut[a,b], Emmanuel Guillot[a], Alexis Vossier[a]

[a] *CNRS, Laboratoire PROcédés, Matériaux et Energie Solaire (PROMES), UPR 8521, 7 Rue Du Four Solaire, 66120, Odeillo, France*
[b] *OSE-Engineering, 1 Route de Versailles, 78470 Saint-Rémi-lès-Chevreuse, France*

Abstract

Do compact Photovoltaic-Concentrated Solar Power hybrid systems offer the opportunity for the expansion of the global solar market? Despite the inherent potential of this technology to provide both affordable and dispatchable solar electricity, it is still unclear how the combination of Photovoltaic and Concentrated Solar Power may offer a net advantage over conventional solar plants. Herein, large-scale compact Photovoltaic-Concentrated Solar Power hybrid plants are modelled considering two different hybrid approaches, over a whole year operation, and compared with a conventional Concentrated Solar Power plant. A detailed optical, electrical and thermal model is developed to analyze the temporal output characteristics of the hybrid plants, based on realistic input parameters and representative meteorological data in Targassonne, France. Results show that both hybrid systems may deliver significantly higher energy output over the conventional Concentrated Solar Power plant, provided that several key parameters are optimized. Furthermore, the sensitivity of the two-hybrid strategies investigated to the operating conditions, and to the characteristics of the solar cells used, are analyzed. In the light of these results, the main scientific and technological issues one should address to ensure optimal operation of these compact hybrid plants are finally discussed.

Keywords:
Photovoltaics, Concentrated Solar Power, compact hybrid systems, annual energy analysis,

1. Introduction

Intense efforts are currently invested around the world to raise the proportion of electricity produced by renewable energies. Up to now, the deployment of solar electricity primarily involved conventional silicon flat plate modules [1]. However, owing to the intermittent nature of the solar resource, ensuring a satisfying balance between the available energy supply and the demand profile remains a challenging issue.

A possible way to tackle this obstacle lies in the marriage between two different solar technologies: first, Photovoltaic (PV) technology, where the solar radiation is directly converted into electricity either through flat PV modules or concentrated solar cells and second, Concentrated Solar Power (CSP) technology, capable of converting sunlight into thermal energy using a Heat Transfer Fluid (HTF) that can be used to store heat for a long duration (1–18 h) when integrated with a Thermal Energy Storage system (TES) [2–11]. Merging these two technologies into one single power plant would thus offer the combined benefit of increased solar-to-electricity efficiency, reduced PV costs and affordable TES, ensuring beyond daytime solar electricity production without the need for expensive and cumbersome electrochemical batteries.

Hybrid PV-CSP systems can be classified into two main families, namely *non-compact* and *compact* systems [2]: the former refers to independently operating PV and CSP plants, usually located close to each other, while the latter combines every strategy involving an amalgamation of the two PV and CSP technologies into one single system.

There is a strong incentive in the development of *compact* hybrid systems: the improved exploitation of the solar spectrum may reduce losses, improve efficiency, as well as cutting down the land footprint, over *non-compact* systems. *Compact* PV-CSP hybrid systems can essentially be subdivided into two main strategies, stemming from different physical principles: 1) the ***High Temperature*** (*HT*) hybrid strategy, which refers to a thermally coupled system where the heat dissipated from the solar cells is recovered using a thermal collector bonded to the PV cells rear face (this approach is also known as Wasted Heat Recovery (WHR) system)[5, 6, 12] and 2) the ***Spectral Beam Splitting*** (*SBS*) approach, involving the family of systems involving a spectral separation of the incoming rays, which are redirected either onto the PV cells or on the thermal receiver, depending on their wavelength. Unlike the first hybrid approach, both subsystems are thermally decoupled, resulting in lower operating temperatures for the PV cells, and thus higher PV efficiencies [13–16]. This last family of *compact* hybrid sys-

E-mail address: alexis.vossier@promes.cnrs.fr (Alexis Vossier)

Nomenclature

$1S$	one-sun
CSP	Concentrated Solar Power
DHI	Diffuse Horizontal Irradiance, $(\mathrm{W/m^2})$
DNI	Direct Normal Irradiance, $(\mathrm{W/m^2})$
E	Photon energy, (eV)
f	Spectral distribution of light, $(\mathrm{W/m^2nm})$
G	Global Irradiation, $(\mathrm{W/m^2})$
GHI	Global Horizontal Irradiance, $(\mathrm{W/m^2})$
h	Convective heat exchange coefficient, $(\mathrm{W/m^2K})$
HT	High Temperature
HTF	Heat Transfer Fluid
J	Current density, $(\mathrm{A/m^2})$
K	Number of time steps
N	Number of heliostats
$NOCT$	Nominal Operating Cell Temperature
P	Power, (W)
PV	Photovoltaic
Q	Cumulative energy, $(\mathrm{GW\,h})$
R	Reflectivity
S	Surface, $(\mathrm{m^2})$
SBS	Spectral Beam Splitting
SPT	Solar Power Tower
T	Temperature, $(^\circ\mathrm{C})$
t	time
TES	Thermal Energy Storage
U	Heat transfer coefficient, $(\mathrm{W/m^2\,K})$
V	Voltage, (V)
v	Velocity, $(\mathrm{m/s})$
WHR	Waste Heat Recovery
X	Concentration ratio of sunlight, (suns)

Greek

α	Absorptivity
α'	Energy gap parameter, $(\mathrm{eV/K})$
β	Temperature coefficient of power, $(\%/\mathrm{K})$
β'	Energy gap parameter, (K)
δ	time step, (min)
η	Efficiency
λ	Wavelength, (nm)
ρ	Reflectivity
τ	Transmittance
θ	Angle, $(^\circ)$
ε	Surface emissivity
ζ	Shockley-Queisser index

Physical Constants

σ	Stefan-Boltzmann constant, 5.67×10^{-8} $(\mathrm{W/m^2K^4})$
c	Speed of light in vacuum, 3×10^8 $(\mathrm{m/s})$
h	Planck constant, 6.62×10^{-34} $(\mathrm{J\,s})$
k	Boltzmann constant, 1.38×10^{-23} $(\mathrm{J/K})$
q	Elementary charge, 1.602×10^{-19} $(\mathrm{A\,s})$

Subscripts

amb	ambiant
blo	blocking
c	cell
$conv$	convection
dif	diffuse
dir	direct
exp	experimental
g	gap
hel	heliostat
in	incident
$loss$	loss
Mir	Mirror
rad	radiative
rec	receiver
ref	reference
sc	short-circuit
sh	shading
$spil$	spillage
sq	Shockley-Queisser
t	total
th	thermal
tra	transmission
$wind$	wind

tems can be subdivided into two groups, based on the nature of the filtering technique used to divert the incoming light: a) reflection-transmission, where the incoming light is spectrally separated after passing through optical filters and b) absorption-transmission techniques based on two main means, nanofluids [17–19] or PV cells [20–22], where a fraction of the incoming sunlight is absorbed by the filters, the rest being either reflected to the PV subsystem or to the thermal receiver, depending on the filtering technique.

The improvement of these *compact* hybrid systems has instigated an increasing interest in the solar community recently, particular efforts being invested in the experimental characterization of the *SBS* hybrid strategy [15, 17, 18, 21, 23]. Conversely, the *HT* approach has essentially been investigated on theoretical grounds, the technological maturity of the *HT* cells required being currently too low to allow any experimental work [5, 6, 24–26].

However, the extent to which *compact* hybrid power plants may outperform conventional solar power plants is still unclear: in practice the combination of two different solar technologies into one single device requires 1) solar cells operating far beyond ambient temperature or 2) optical components precisely diverting sun rays onto the PV cells or the thermal receiver, depending on their wavelength. Each of these components may constitute the Achilles' heel of the strategy in which they are involved, raising the need for a better understanding of the constraints these components should fulfill toward ensuring superior performances over conventional solar plants. In a previous attempt to better evaluate the performance of the main hybrid strategies, it was shown that *compact* hybrid systems are likely to slightly surpass conventional solar plants when considering ideal operating conditions (i.e. perfect cutoff of the optical components, ambient temperature assumed equal to 298 K, incident solar power of 1000 $\mathrm{W/m^2}$) together with close to ideal operation of PV cells, thermal receiver, and turbines [27, 28]. However, a benchmark of the different *compact* hybrid strategies on the sole basis of the net solar-to-electricity efficiency is questionable: it is complicated to compare different strategies relying on different physical principles and using different solar inputs (direct solar irradiance for the *HT* strategy, global solar irradiance for the approaches involving PV cells as spectrum separator) is indeed rather intricate, especially with the simplified assumptions used regarding their operation. In this work, we aim to clarify this question by developing an accurate physical and optical model of the main *compact* hybrid strategies, based upon their integration in a real solar power plant. THEMIS central receiver demo-plant (shown in Figure 1), was selected as a case study owing to the large number of technical and meteorological data available on-site. Despite the recent interest in hybrid systems involving only PV and TES (the TES being heated by an electrical resistor fed by PV electricity [29]), we restrict this comparative work to hybrid plants involving solar power towers, for the sake of consistency.

First, we begin with a description of THEMIS plant, and by a reminder of the main optical and physical laws applying to each candidate strategy considered in this work. Then the energy output analyses are carried out under real operating weather conditions (irradiation, temperature, wind velocity) over a whole year, and considering different time resolution. Third, we evaluate the effects of several parameters on the energy output of the different strategies. In the light of these results, we finally discuss the main key-challenges to be overcome for each strategy, in order to guarantee an optimal energy output.

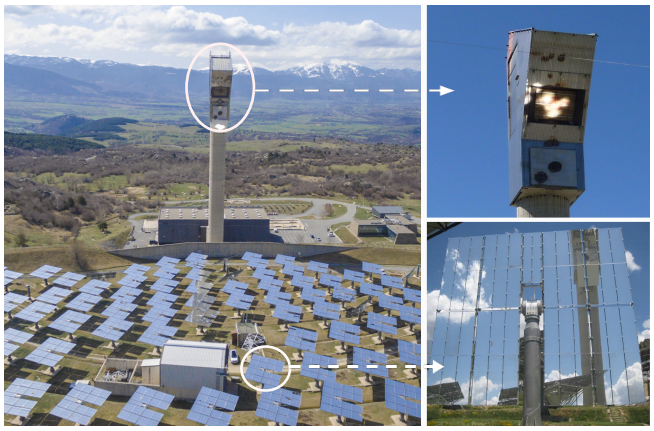

Figure 1: **THEMIS** Solar Power Tower with a close look at the central receiver at the top of the tower and one of the heliostats in the solar field.

2. System description

THEMIS Solar Power Tower (SPT) is a 5 MW_{th} R&D facility located in Targassonne, in Southern France, with a solar resource approaching 2150 $\mathrm{kWh/m^2/year}$ of direct normal irradiation (DNI). The heliostats field at THEMIS has 107 heliostats (cf. Figure 1) each composed of nine modules (i.e. set of mirrors): eight modules of 3.62 m x 1.79 m, and one module of 2.46 m x 0.83 m filling the central gap left by the tracking system, as shown in Figure 2(a). The solar tower is 100 m high, and the receiver is located 86 m above ground level [30–32]. For the purpose of this work, the dimensions of the open receiver are set equal to 4 m x 2 m. Table 1 lists the most important characteristics of THEMIS plant considered in this study.

Here, we aim to compare the performance of two families of hybrid strategies with the type of conventional CSP plant THEMIS was originally designed for. Each candidate strategy implies a modification of either the receiver (*HT* strategy) or the heliostat field (*one-sun* hybrid system), described hereafter.

2.1. One-sun hybrid system

The ***one-sun (1S)*** PV-CSP hybrid system considered in this work is basically inspired from Holman et al. [20–22], and is schematically depicted in Figure 2(a). The mirrors used in the heliostat field are replaced by PV cells including a back reflector, thus allowing sub-bandgap photons to be reflected onto the thermal receiver. We assume GaAs PV cells from Alta Devices (that currently hold the world record for single-junction solar

cells [33]) to be integrated onto the heliostats. The fraction of incident solar power absorbed by the PV cells (~ 65%) is calculated from the spectral reflectance curve represented in Figure 2(b), the remaining fraction being sent onto the receiver. Unlike other hybrid strategies, the *1S* approach offers the inherent advantage of converting a large fraction of the diffuse light (the solar resource available for each PV heliostat at every time step will be described in detail in the next section).

2.2. HT hybrid system

Unlike the ***1S*** strategy, the ***HT*** approach does not involve any modification of the heliostat field, but uses PV cells as the outer part of an integrated receiver, thermally bonded to a thermal receiver beneath it, as depicted in Figure 3. The heat generated by sub-bandgap photons and thermalised electrons is transferred to the HTF, which is assumed to be at a temperature of 400 °C (a value coherent with the first long-duration characterizations of HT PV cells [34]).

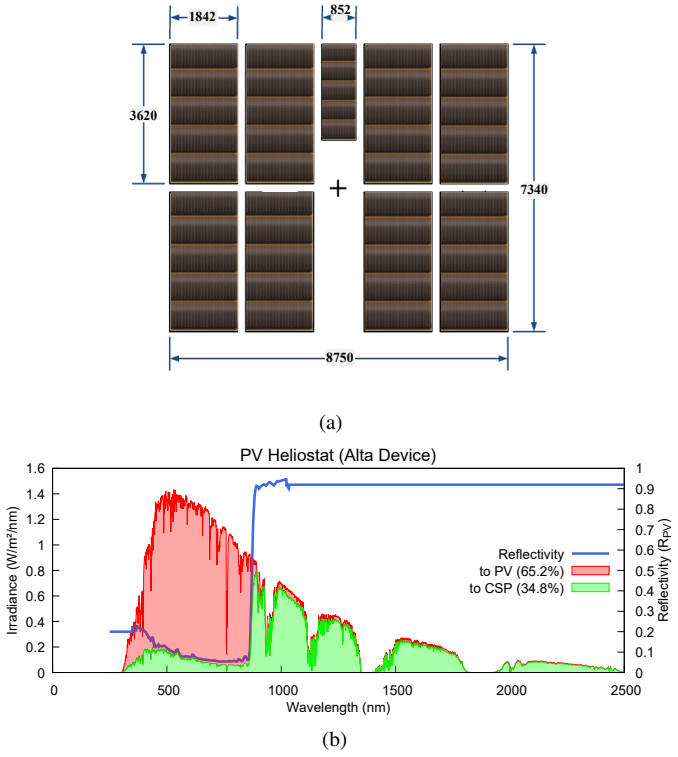

Figure 2: (a) Schematic of a PV heliostat used in the *1S* hybrid system, (b) Spectral distribution of solar radiation and spectral reflectance of GaAs solar cell (blue: cell reflectivity [35], red: power absorbed by PV, green: power sent to CSP).

3. Model description

We developed a predictive model providing the energy output for each strategy, on an annual basis, in order to compare the performance of these two-hybrid technologies with THEMIS conventional CSP plant. The model takes as inputs:

- The geographical coordinates for the location of interest (altitude, longitude, latitude),
- The local time,
- Several important meteorological parameters: temperature, wind velocity, and irradiation data (direct, diffuse and global). The latter were measured on-site considering one almost-complete year (2018): the missing and low-quality data (8 days out of 365 days) were replaced with equivalent irradiation data measured during previous years. These data were selected after identifying similar days (DNI energy level and variation), and were implemented in the data-set following the procedure described in [36],
- The position of the heliostats regarding each other and the tower as well as the main characteristics of the receiver.

The model calculates the sun's position at every time step throughout the year, along with the heliostat field efficiency (taking into account cosine, shading and blocking losses). The power absorbed and reflected by each individual heliostat is then calculated, considering the spectral reflectance $R_{PV}(\lambda)$ measured over the solar spectrum curve ($\lambda = 250-2500$ nm) of the GaAs cells [35] used as PV heliostats in the *1S* approach (cf. Figure 2(b)) or a mean mirror reflectivity value of 90% (*HT* approach and CSP). The electrical and thermal output of the PV and CSP subsystems are calculated applying a set of equations (*vide infra*) describing the optical, electrical and thermal behaviour of each strategy investigated. The annual energy output is finally calculated for two different time steps 1 and 5 min. The following assumptions are adopted in the model:

1. Both the high-temperature solar cells and the HTF are supposed to be at a fixed temperature of 400 °C.
2. ***GaAs*** single-junction solar cells are employed in both hybrid systems.
3. The receiver is described by a set of basic parameters (temperature, absorptivity, emissivity, and convective heat loss coefficient), without specifying any particular material, geometry, or coating.
4. No TES is considered in this first analysis. Nevertheless, the object of the concept is obviously to store the heat energy collected by the thermal receiver in order to produce power after sunset.

Table 1: **THEMIS** power plant input parameters of the model.

Heliostat field	
Number of Heliostats N_{hel}	107
Reflective area, S_{hel}	53.7 m^2
Mirror reflectivity, ρ_{Mir}	0.9 [30]
Central Receiver	
Area, S_{rec}	8 m^2
Temperature, T_{rec}	400 °C
Absorptivity, α	0.95
Surface emissivity, ε	0.9
Convective heat loss coefficient, h_{conv}	10 W/m^2K

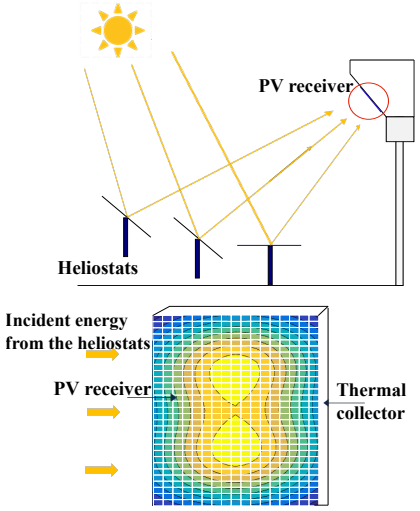

Figure 3: Schematic of the *HT* hybrid approach with a close look at the PV receiver entirely covered with solar cells (represented by the white squares).

In the following paragraphs, the model is described in detail. All input parameters of the model are listed in Tables 1, 2 and 3.

3.1. Optical model

The instantaneous optical efficiency of the heliostat field accounts for different loss mechanisms depicted in Figure 4(a), and calculated as [4]:

$$\eta_{hel} = \rho\, \eta_{tra}\, \cos\theta\, \eta_{sh}\, \eta_{blo}\, \eta_{spil} \tag{1}$$

where ρ refers to the heliostat reflectivity, the value of which depends on the type of system considered, η_{tra} is the atmospheric transmission between the heliostat and the receiver (which is assumed equal to 1 in this study), while $\cos\theta$, η_{sh}, η_{blo} and η_{spil} are the main sources of optical losses in the heliostat field: $\cos\theta$ is the cosine of the angle formed between the normal to the heliostat surface and the incident rays, η_{sh} is the fraction of the heliostat surface shaded by adjacent heliostats, η_{blo} is the fraction of the reflected sunlight blocked by adjacent heliostats, and η_{spil} refers to the fraction of reflected sunlight missing the receiver due to heliostat tracking errors, unsuitable aiming strategies, non-specular reflection on the heliostat, etc...
SolarPILOT software [37] was used to precisely characterize the optical performance of the heliostat field, using as an input the positions of the sun and the heliostats along with the receiver characteristics. As an example, Figure 4(b) represents the total efficiency of THEMIS heliostats field on the 21st December at noon. The grey area represents the shadow of the heliostat field along the direction of the sun position. These results illustrate the fact that heliostats located on both edges of the solar field are less efficient, as a consequence of their orientation relative to the receiver.

3.1.1. One-sun approach

In this strategy, the heliostat reflectivity is calculated as the ratio between 1) the power reflected by the PV heliostat, computed as the integration of the spectral reflectivity of the PV mirrors multiplied by the spectral distribution of sunlight over the solar range (250-2500 nm) and 2) the total solar power impinging the heliostats (i.e the integration of the spectral distribution of sunlight over the solar range):

$$\rho_{1S} = \frac{\int_{250}^{2500} R_{PV}(\lambda) f(\lambda) d\lambda}{\int_{250}^{2500} f(\lambda) d(\lambda)} \tag{2}$$

where $f(\lambda)$ refers to the spectral distribution of the incoming sunlight (λ being the wavelength of solar radiation, expressed in nm).

The optical power sent onto the receiver by the heliostat field is calculated as the sum of the optical power sent by each PV heliostat. The total optical power at a given time t can then be computed as:

$$P_{rec,1S}(t) = \sum_{i=1}^{N_{hel}} \eta_{hel,1S}(t) S_{hel} DNI(t) \tag{3}$$

3.1.2. HT approach and CSP

For both the *HT* approach and the conventional CSP plant, the reflectivity of each heliostat is taken equal to the mirror reflectivity:

$$\rho_{HT} = \rho_{CSP} = \rho_{Mir} \tag{4}$$

and the total optical power sent onto the receiver is calculated as:

$$P_{rec,HT}(t) = P_{rec,CSP}(t) = \sum_{i=1}^{N_{hel}} \eta_{hel,Mir}(t) S_{hel} DNI(t) \tag{5}$$

3.2. Electrical model

For a precise estimation of the PV output of the system, one has to take into account the temperature and illumination dependence of the PV technology used. In the detailed balance limit [38] the current-voltage curve of an ideal PV cell can simply be deduced from the equation:

$$J(V) = J_{sc} - J_{rad}(V) \tag{6}$$

where J_{sc} is the short-circuit current density, while $J_{rad}(V)$ is the diode current, stemming from radiative recombination occurring in the cell. J_{sc} can be written as:

$$J_{sc} = q\, X \int_{250}^{\lambda_g} f(\lambda)\, d\lambda \tag{7}$$

where q is the elementary charge and X is the concentration ratio of sunlight.

The radiative recombination current density is calculated in

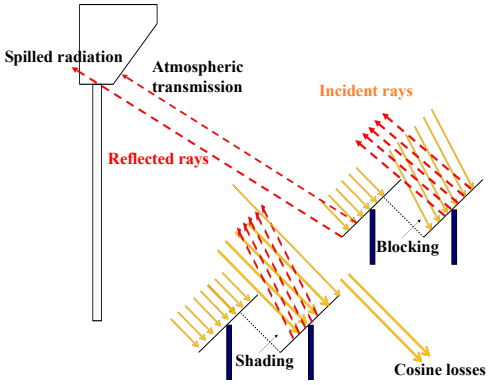

(a)

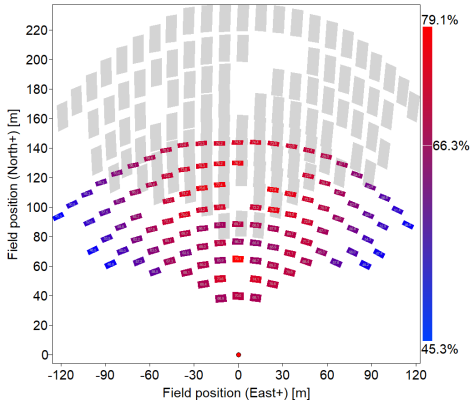

(b)

Figure 4: (a) Schematic description of the main optical losses of the heliostat field, (b) SolarPILOT plot showing THEMIS heliostat field overall efficiency.

the detailed balance limit as [38]:

$$J_{rad}(V) = \frac{2\pi}{h^3 c^2} \int_{E_g}^{\infty} \frac{E^2\, dE}{\exp\left(\frac{E - qV}{kT_c}\right) - 1} \tag{8}$$

where h and k are respectively the Planck and Boltzmann constants, c the speed of light and E_g the bandgap of the PV cell used. E refers to the energy of photons, while T_c is the temperature of the PV cells, which value is a function of the strategy considered. Because of the wide range of operating temperature considered in this work, one has to take into account the temperature dependence of the bandgap, which can be described by the following equation [39]:

$$E_g(T) = E_g(0\ \mathrm{K}) - \frac{\alpha' T^2}{T + \beta'} \tag{9}$$

where α' and β' are material dependent constants, whose values are reported in Table 2. Finally, the PV efficiency is simply calculated as the ratio between 1) the maximum electrical power extractable from the PV cell (referred as the maximum power point, i.e. the maximal value of the product between the voltage V applied to the cell and the current density $J(V)$) and 2) the incident solar power P_{in} absorbed by the PV receiver , the value of which is a function of the strategy considered:

$$\eta_{PV} = \frac{max\left[V \times J(V)\right]}{P_{in}} \tag{10}$$

Providing a realistic estimate of the electric production of the PV modules, rather than an idealized one, requires this model to be altered to better describe the cell technology considered. Each candidate technology involves GaAs operating on vastly different ranges of temperature and illumination. The electrical model is thus adapted to each strategy, and the assumptions pertaining to each strategy will be described in the following subsections.

3.2.1. *One-sun approach*

The PV output in the *1S* approach is calculated assuming that the PV efficiency is independent of the DNI (a specific calculation shows that the gap in PV efficiency between the extreme DNI values throughout the year, ranging from 300 $\mathrm{W/m^2}$ to 1094 $\mathrm{W/m^2}$, is less than 0.1 % absolute). The temperature dependence of the PV cell efficiency is estimated applying the following equation [4]:

$$\eta_{1S}(T_c) = \eta_{ref}\ \left[1 + \beta_{ref}\left(T_c - T_{ref}\right)\right] \tag{11}$$

where η_{ref} refers to the reference PV efficiency in standard test conditions, calculated by solving Eq.(10), β_{ref} is the *GaAs* temperature coefficient, while T_c and T_{ref} are the cell and reference temperatures. The cell temperature is calculated as a function of the meteorological parameters using [4]:

$$T_c = T_{amb} + (T_{NOCT} - T_{a,NOCT})\,\frac{GHI}{G_{NOCT}}\,\frac{U_{NOCT}}{U}\left(1 - \frac{\eta_{1S}}{\tau\alpha}\right) \tag{12}$$

where T_{amb} is the ambient temperature, $(\tau\alpha)$ is the effective transmittance-absorptance of the PV module, U the heat transfer coefficient, calculated using the equation reported in Table 2 where v_{wind} is the wind velocity, GHI the global irradiation, U_{NOCT} and G_{NOCT} the heat transfer coefficient and the global irradiation at the nominal operating cell temperature (NOCT) given in Table 2.

A precise estimation of the solar resource impinging each heliostat should take into account that 1) each heliostat does not strictly face the sun, but is rather positioned at mid-angle between the sun and the receiver located at the top of the tower 2) PV heliostats offer the inherent advantage of converting a fraction of diffuse sunlight, which is function of the panel orientation.

The direct solar power impinging each individual PV heliostat can then be written:

$$P_{dir}(t) = S_{hel} cos\theta(t) \eta_{blo}(t) \eta_{sh}(t) DNI(t) \tag{13}$$

The diffuse solar power intercepted by each heliostat at a

given time t is [40]:

$$P_{dif}(t) = \frac{[1 + cos\beta(t)]}{2} S_{hel} DHI(t) \quad (14)$$

where β is the angle formed between the normal to each individual heliostat and the ground, and DHI is the Diffuse Horizontal Irradiance. The total PV power generated at a given time t can thus be calculated as:

$$P_{PV,1S}(t) = \sum_{i=1}^{N_{hel}} \zeta_{SQ,1S}\, \eta_{1S}(t)\, [P_{dir}(t) + P_{dif}(t)] \quad (15)$$

where $\zeta_{SQ,1S}$ translates the ability of a given cell technology to approach its own theoretical limit [41], and will be detailed in section 3.2.3.

Table 2: Main parameters of the PV cell used in both hybrid approaches.

Reference operating conditions	
Temperature coeff. of power, β_{ref}	-0.08 %/K [42]
Reference temperature, T_{ref}	25 °C
U= $5.67 + 3.86\, V_{wind}$	
$\tau\,\alpha$	0.85 [43]
NOCT conditions [44]	
T_{NOCT} = 46 °C	$T_{a,NOCT}$ = 20 °C
U_{NOCT} = 9.53 W/m^2 K	G_{NOCT} = 800 W/m^2
Energy bandgap parameters [39]	
$E_g(0\ \mathrm{K})$	1.519 eV
α'	5.405×10^{-4} eV/K
β'	204 K

3.2.2. HT approach

The *HT* strategy implies radically different operating conditions for the PV cells: we assume that the cell temperature is kept constant and equal to 400 °C. Practically, adjusting the HTF flow rate to the incoming concentrated solar power should allow this condition to be satisfied (it should also be pointed out that the temperature dependence of PV cells has been shown to decrease significantly with sunlight concentration, relaxing the need for a rigorous temperature dependence which accounts for the variations in the operating temperature the PV receiver may be exposed to in reality [34, 45]).

The PV efficiency in the *HT* approach is thus calculated as a function of temperature and sunlight concentration solving Eq.(10), assuming a cell temperature of 400 °C and a concentration ratio of sunlight given by:

$$X(t) = \frac{P_{rec,HT}(t)}{1000 \times S_{rec}} \quad (16)$$

The PV output is finally calculated as:

$$P_{PV,HT}(t) = \zeta_{SQ,HT}\, \eta_{HT}(t)\, \eta_{th}(t)\, P_{rec,HT}(t) \quad (17)$$

where η_{th} is the thermal efficiency, which will be described in more detail in section 3.3, while $\zeta_{SQ,HT}$ translates the ability of a realistic *HT* cell technology to approach its own theoretical limit.

3.2.3. From ideal to realistic solar cells

Realistic PV cells are likely to be affected by several limiting mechanisms (series resistance losses, non-radiative recombination, imperfect absorption...) which prevents them from achieving the ideal efficiency derived previously in the radiative limit. To better account for these losses, we choose to alter the PV model by introducing a corrective coefficient, referred to as ζ_{SQ}, translating the ability of a given cell technology to practically approach its own theoretical limit [41]:

$$\zeta_{SQ} = \frac{\eta_{PV,exp}}{\eta_{PV,SQ}} \quad (18)$$

where $\eta_{PV,exp}$ is a realistic efficiency value measured experimentally, while $\eta_{PV,SQ}$ is the theoretical upper limit for the corresponding PV cell technology. This fixed parameter is thus used as a way to quantify how a particular cell technology will deviate from the ideal PV efficiency, because of internal loss mechanisms (the dependence on external operating conditions, such as temperature or illumination, being taken into account in the model, as described previously). Typical values of ζ_{SQ} may vary considerably, depending on the cell technology or the operating conditions to which the cells are submitted experimentally. We have selected GaAs as a PV cell technology. On the one hand, GaAs has been proven to experimentally reach very high conversion efficiencies, currently exceeding 29% under one-sun conditions [33], making this cell technology a good candidate for approaching unity values of ζ_{SQ} under one-sun operation. On the other hand, experimental data regarding the high-temperature operation of GaAs cells remain scarce, and the rare experimental characterizations of comparable cell technologies show ζ_{SQ} values of ~ 0.35 [34, 45]. To explore the impact of the PV cell efficiency on the performance of the hybrid system, we thus select 3 different values of ζ_{SQ} for each strategy considered, corresponding to 3 operational scenarios. Because there is a huge gap in the industrial maturity of these cell technologies (high-temperature solar cells are still in their infancy, while conventional one-sun GaAs solar cells had the benefit of decades of research and development, culminating in the 29.3% world-record efficiency for single-junction solar cells), the ζ_{SQ} value associated with each of these scenarios varies depending on the strategy considered:

- **Optimistic scenario**:
  - *One-sun approach*: The PV efficiency is assumed to be equal to the record GaAs *cell* efficiency reported in the literature [46], leading to ζ_{SQ} of 0.9.
  - *HT approach*: We assume a similar ζ_{SQ} value of 0.9, with a corresponding experimental efficiency of ~ 30%.
- **Realistic scenario**:

  - *One-sun approach*: The PV efficiency is taken to be equal to the record GaAs *module* efficiency reported in the literature [47], leading to ζ_{SQ} of 0.76.
  - *HT approach*: We assume ζ_{SQ} = 0.65, a median value between the optimistic and pessimistic ζ_{SQ} values considered in this work.

- **Pessimistic scenario**:
  - *One-sun approach*: The PV efficiency is taken equal to the experimentally measured efficiency of large dimension SunPower Silicon flat panels [47]. This scenario thus accounts for a possible degradation in the typical efficiency of mass-produced, large-scale PV modules, leading to ζ_{SQ} of 0.7.
  - *HT approach*: We assume the use of *HT* PV cells with efficiencies equivalent to the one reported in previously published experimental work [27, 34], leading to a ζ_{SQ} value of 0.4.

The ζ_{SQ} indices associated with each scenario considered are reported in Table 3, together with the corresponding experimental efficiencies.

Table 3: Summary of the ζ_{SQ} values considered in this work for the two hybrid strategies investigated, considering GaAs solar cell.

One-sun approach	$\zeta_{SQ,1S}$	$\eta_{PV,exp}$	Reference
Optimistic scenario	0.9	29.3%	[46]
Realistic scenario	0.76	25.1%	[47]
Pessimistic scenario	0.7	22.8%	[47]
HT approach	$\zeta_{SQ,HT}$	$\eta_{PV,exp}$	Reference
Optimistic scenario	0.9	29.7%	”
Realistic scenario	0.65	21.45%	”
Pessimistic scenario	0.4	13.2%	[27, 34]

3.3. Thermal model

The thermal exchanges are modelled assuming convective and radiative heat losses between the receiver surface and the environment (the other sides of the receiver are supposed to be perfectly insulated, and the heat conduction losses are neglected). The thermal efficiency of the receiver is calculated as [48]:

$$\eta_{th}\, P_{rec}(t) = \alpha\, P_{rec}(t) - P_{loss} \tag{19}$$

$$\eta_{th}(t) = \alpha - \frac{\overbrace{\varepsilon\,\sigma\, S_{rec}\,(T_{rec}^4 - T_{sky}^4)}^{P_{rad}} + \overbrace{h_{conv}\, S_{rec}\,(T_{rec} - T_{ref})}^{P_{conv}}}{P_{rec}(t)} \tag{20}$$

where P_{loss} is the power loss due to convection and radiation (=P_{rad} + P_{conv}), α, ε and σ are the absorptivity, the surface emissivity, and Stefan-Boltzmann constant, while h_{conv} is the convective heat transfer coefficient, computed using the physical properties of air [49], and T_{sky} is the sky temperature (calculated as $= 0.0552\,(T_{amb})^{1.5}$). If the numerator of this equation does not basically depend on the strategy considered, the thermal efficiency is also function of the optical power sent onto the receiver by the heliostats field. Consequently, η_{th} will necessarily vary significantly depending on the approach investigated, the optical power in the *1S* strategy ($P_{rec,1S}$) being noticeably lower than the corresponding optical powers in the *HT* ($P_{rec,HT}$) and conventional CSP approaches ($P_{rec,CSP}$). The nominal turbine power is calculated based on the optical power reflected by the heliostat field on the 21^{st} March, at noon, and is equal to 690 kW for both the *HT* approach and the conventional CSP turbine, and 250 kW for the 1*S* approach. There is a minimum thermal power value below which the turbine is assumed not to operate. In practice, this threshold value corresponds to the minimum power required for the turbine to efficiently operate, and the corresponding DNI value is set here to 300 $\mathrm{W/m^2}$ [50]. The electrical power generated by the turbine is calculated assuming a turbine operating at 2/3 of the Carnot limit (an assumption practically describing the operation of realistic turbines [51]). The Carnot efficiency η_{Carnot} is calculated based on the thermal stream operating temperature T_{rec} and assuming a constant cold reservoir temperature T_{ref} of 25 °C:

$$\eta_{Carnot} = 1 - \frac{T_{ref}}{T_{rec}} \tag{21}$$

The electrical power generated by the turbine can be estimated in the *1S* and CSP approaches using Eqs.(22) and (23):

$$P_{CSP,1S}(t) = \frac{2}{3}\,\eta_{Carnot}\,\eta_{th}(t)\,P_{rec,1S}(t) \tag{22}$$

$$P_{CSP,CSP}(t) = \frac{2}{3}\,\eta_{Carnot}\,\eta_{th}(t)\,P_{rec,CSP}(t) \tag{23}$$

The use of an integrated receiver in the *HT* strategy requires the PV power produced by the *HT* receiver to be subtracted from the optical power sent by the heliostats field in order to estimate the thermal power, as described in Eq. (24):

$$P_{CSP,HT}(t) = \frac{2}{3}\,\eta_{Carnot}\,\left[\eta_{th}(t)\,P_{rec,CSP}(t) - P_{PV,HT}(t)\right] \tag{24}$$

3.4. Energy calculation

The energy flows associated with the different contributions discussed previously are simply calculated as a summation over a whole year:

$$Q_i = \sum_{t=1}^{t=K_t} P_i(t)\,\delta(t) \tag{25}$$

where P_i refers to the power associated with the parameter of interest at a given time t, $\delta(t)$ is the time step (either 1 or 5 minutes) and K_t is the total number of time steps over the year (K_t=525600 for $\delta(t) = 1$ min, 105120 for $\delta(t) = 5$ min). The disparity observed in the results being systematically less than 2 %, and because of the significant increase in the calculation time associated with the 1 min time-step (from ∼1.5 days per

calculation with a 5 min time-step against ~5 days with a 1 min time-step), we select a default time resolution of 5 minutes in the rest of this work. The nature of the solar plant considered in this study precludes any global validation of the model since 1) THEMIS power plant was used as a solar facility delivering electricity to the grid but no operation data is available that would have allowed a direct solar-to-electricity validation 2) the key components of the hybrid strategies investigated here are currently not mature enough to be integrated into an operational power plant. The validation for the optical and the electrical models are provided in the supplementary material.

4. Results & Discussion

4.1. Daily performance

The variation of the power output for the hybrid strategies and the conventional CSP plant are shown in Figure 5, along with the DNI profile, and for two representative days. April 17^{th} (Figure 5(a) and 5(b)) corresponds to a clear-sky day, showing smooth variations of the DNI throughout the day, while June 17^{th} (Figure 5(c) and 5(d)) is characterized by rapid and abrupt variations of the DNI. It can be noticed that:

- The daily power generation of both hybrid strategies exceed that of the conventional CSP plant, regardless of the meteorological conditions. However, it is worth noticing that the hybrid strategy showing the best performances over conventional CSP plants depends on the DNI pattern. While the *HT* approach demonstrates the best performance during clear-sky days (with an improvement in the power output of 24.5 $\%$ relative to the CSP power output), the *1S* approach shows the highest performance during cloudy days (with an increase in the power output of 25.3 $\%$ relative to the CSP power output), as a result of the improved ability of the PV heliostats to cope with the variable solar resource (the turbine operation being penalized by intermittent stops and starts for DNI values close to 300 $\mathrm{W/m^2}$).
- Because of the existence of a threshold DNI value below which the turbine is assumed not to operate, the response of the different plants to the daily variation of DNI differs noticeably. This translates into an extended operation time of the *1S* approach over the course of the day, due to the increased capacity of the PV heliostats to convert low-power solar radiation close to sunrise or sunset.

Figure 6 shows the electric energy output distribution of the 3 strategies investigated here, as a function of the DNI value and over the course of a year, in Targassonne. As observed above, the electrical output changes noticeably depending on the solar irradiance value: the higher the DNI, the higher the fraction of the total electrical energy produced by the CSP converter. This suggests that the DNI distribution of a particular site over a year should provide useful indications regarding the most appropriate hybrid strategy to be implemented in any particular location.

4.2. Annual performance

4.2.1. Effect of PV cell performances

Figure 7 shows the distribution of the annual energy output for the two-hybrid systems as well as for the conventional CSP plant, and for the 3 operational scenarios described above.

Regardless of the operational scenario considered, we observe a noticeable difference between the energy output of the hybrid strategies, and the energy output of THEMIS conventional plant, with a relative gain in energy ranging from 20% (in the case of the *HT* approach in the pessimistic scenario) to 55% (*1S* approach in the optimistic scenario). These numbers confirm the intrinsic superiority of the two *compact*-hybrid approaches investigated over conventional CSP plant, owing to the increased capacity of the *1S* approach to convert diffuse radiation (the extra-energy output associated with the conversion of diffuse solar radiation representing $\sim 414\mathrm{MW\,h}$ (14%) over a full-year operation), and the improved ability of the *HT* approach to efficiently use high-energy photons (which are commonly wasted and released into the environment, in conventional PV systems).

The two-hybrid strategies demonstrate opposite trends regarding the share between PV and CSP production, suggesting that the nature of the PV cells, the operating conditions to which they are exposed, and their ability to practically approach their own theoretical limits, has tremendous effects on the performance of the hybrid systems. Increased PV efficiency obviously leads to higher system performance, independent of the hybrid technology considered. However, in the *1S* strategy, the improvement in the PV cell efficiency induces a net increase in the PV output without affecting the CSP operation, which translates into very modest changes in the share between PV and CSP depending on the operational scenario considered. Conversely, the improvement in the PV cell efficiency in the *HT* approach simultaneously leads to a net increase in the power output, together with a significant change in the balance between the energy output of the two converters. This speculative scenario is based upon a dramatic improvement in the *HT* cell technology and will require numerous technological and scientific barriers (that will be discussed into details in the final section) to be overcome. It should also be stressed that the amount of thermal losses at the receiver level appears to be significantly lower in the *1S* strategy, as a consequence of the prevalence of reflection losses, that scale proportionally to the optical power sent to the receiver.

The choice of the PV cell technology may alter dramatically these first conclusions, the amount of optical power absorbed by each converter (in the *1S* approach) or the PV temperature dependence (in the *HT* approach) being correlated to the electronic gap of the PV cell. Figure 8 shows the energy fluxes associated with the two-hybrid strategies assuming AlGaInP solar cells as PV converters, and considering a realistic operational scenario (with ζ_{SQ} values estimated following similar assumptions as the ones formulated in the case of GaAs (see Table S1 for the exact numerical values, as well as the corresponding references supporting them)). For improved clarity, the energy shares associated with hybrid plants involving GaAs solar cells

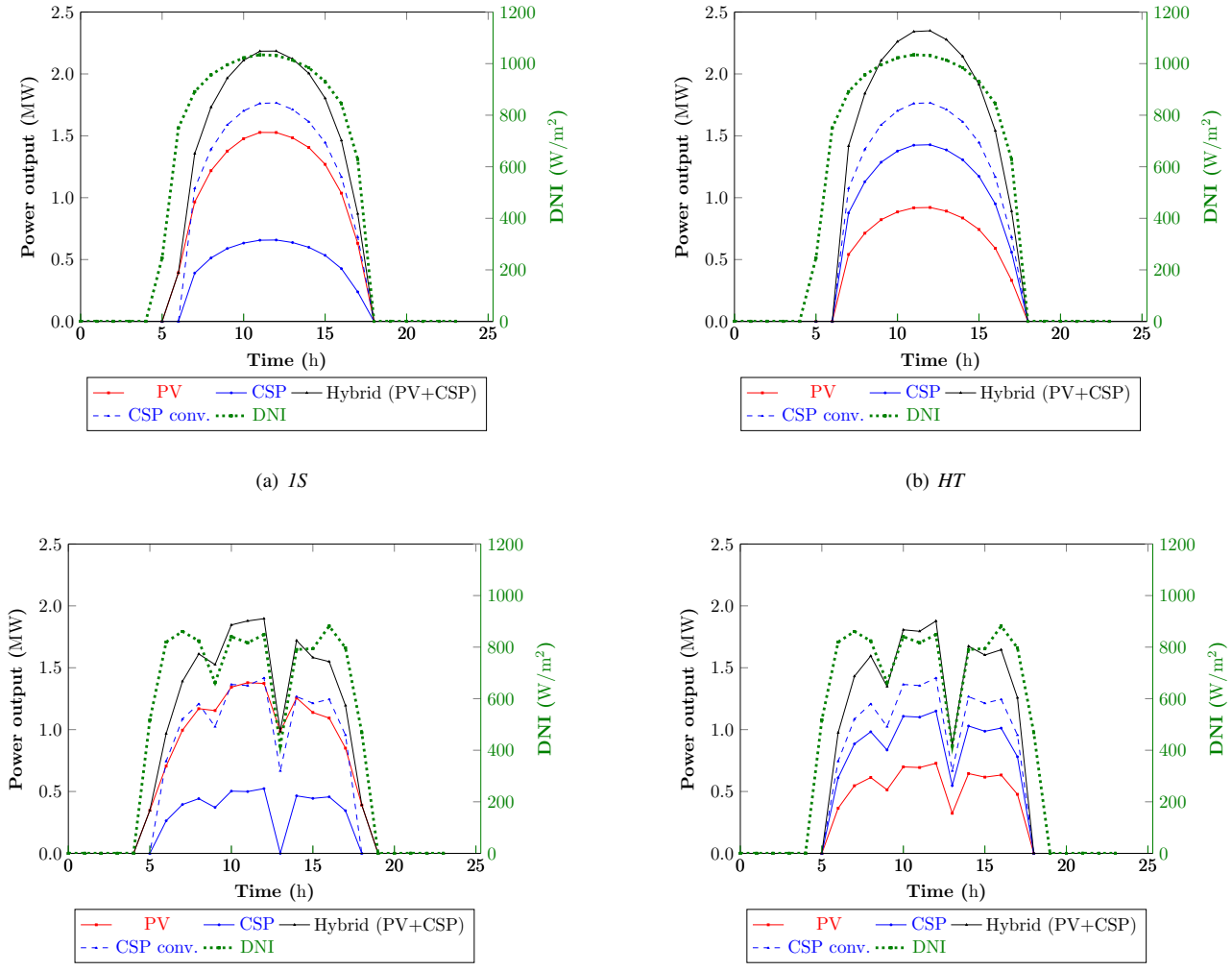

(a) *1S* (b) *HT*

(c) *1S* (d) *HT*

Figure 5: Daily power output variation and DNI profile for the two hybrid strategies considering a time resolution of 60 min, for a clear-sky day (April 17^{th}): (a) and (b), and for a cloudy day (June 17^{th}): (c) and (d).

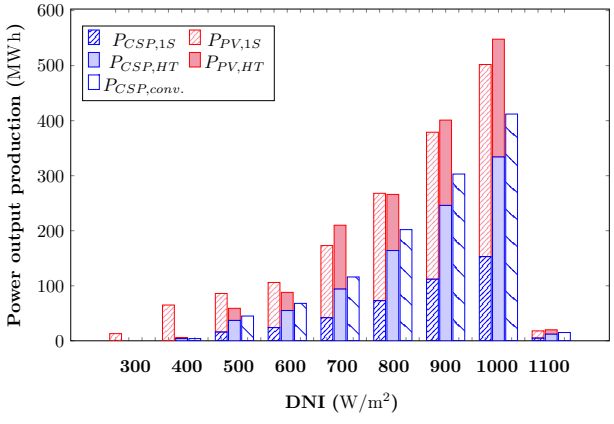

Figure 6: Variation of the power output as a function of DNI, for the two hybrid strategies & THEMIS conventional CSP plant.

are also represented. The numerical values corresponding to the energy fluxes in the pessimistic and optimistic scenarios are reported in Table S3.

If opting for a high-bandgap material as PV cell technology in the *1S* approach leads to an improved balance in the energy output of each converter, it is worth noticing that the total energy delivered by the system is noticeably lower in comparison with hybrid systems involving GaAs solar cells. In the *HT* approach, the use of high-bandgap cells deteriorates both the total energy output of the system and the balance between CSP and PV, relative to the GaAs case, suggesting that the improved temperature resistance of such material does not allow counterbalancing its fundamentally lower efficiency under 1 sun condition.

4.2.2. *Effect of the HTF operating temperature*

The operating temperature of the thermal receiver constitutes a key parameter, affecting the amplitude of thermal losses, the turbine efficiency, as well as the PV output in the *HT* approach involving a PV module acting as a thermal receiver. Figure 9 shows the different energy fluxes associated with the three

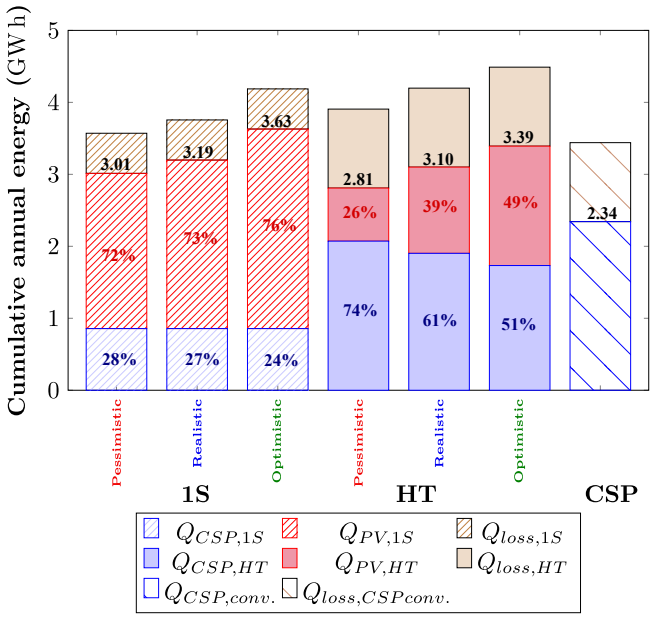

Figure 7: Annual cumulative energy production for the two hybrid approaches & THEMIS conventional CSP plant, considering the pessimistic, realistic, and optimistic operation scenarios.

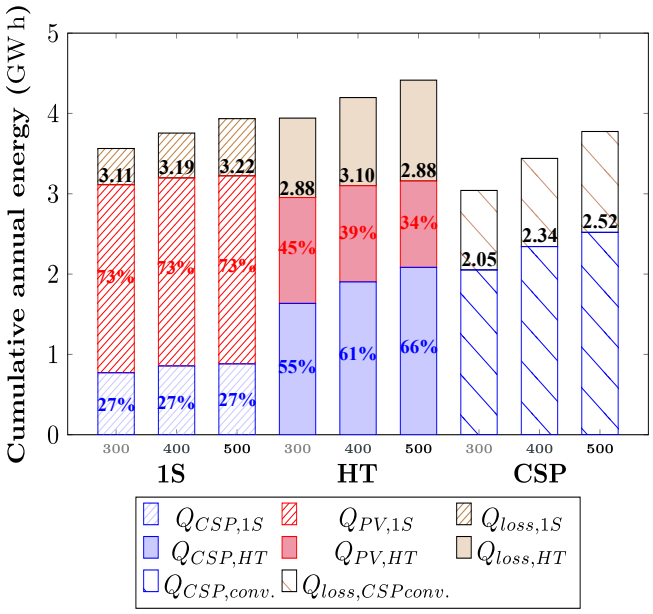

Figure 9: Annual cumulative energy production for the two hybrid approaches & THEMIS conventional CSP plant, in the realistic operation scenario, and for different temperature of the HTF.

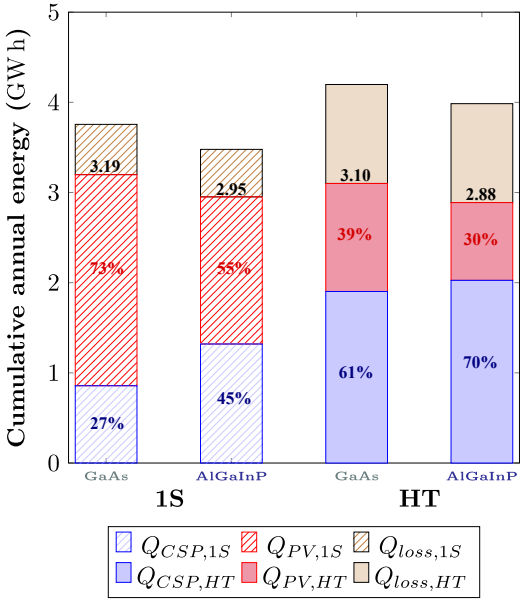

Figure 8: Annual cumulative energy production for the two hybrid approaches, considering the realistic operation scenario, and for two different cell technologies.

strategies investigated, considering a turbine inlet temperature of 300, 400 and 500 °C, and assuming a realistic operational scenario (the numerical values for the other operational scenarios being reported in Table S3).

Overall, the energy output for the three systems considered here increases steadily with increasing temperature. However, the temperature dependence of the energy output changes noticeably depending on the approach: while conventional CSP plants show an improvement in the energy output approaching 23% between 300 and 500°C, the net gain in energy output appears to be far more modest with the two-hybrid approaches (respectively 3.5 and 7 % with the *1S* and *HT* strategies). As a result, the benefit associated with *compact*-hybrid strategies over the conventional CSP plant decreases as the operating temperature is increased (the net gain in energy between *compacts* and CSP plants shifting from ~50% to less than 25 % in this temperature range). The underlying reasons explaining these trends are however different: the global temperature dependence of an integrated PV-CSP receiver stems from the competing temperature dependence of the PV and CSP converters: while the efficiency of the thermal converter increases with turbine inlet temperature, the PV output drops, principally because of the detrimental effect of temperature on V_{oc}, resulting in a less favorable temperature dependence relative to the conventional CSP plant. On the contrary, the decoupling between PV and CSP in the *1S* approach does not induce any penalty in the PV output for increasing turbine inlet temperature. However, the use of PV heliostats in the *1S* approach implies that only a fraction of the incident solar power is sent onto the receiver: the gain in the energy output with increasing temperature thus scales with the fraction of the incident power absorbed by the thermal receiver.

5. Conclusion

In this work, we have developed a rigorous optical, electrical, and thermal model of the main *compact* hybrid strategies, based upon their integration in a real solar power plant. Our motivation here was to assess precisely the performance of the main candidate hybrid PV-CSP strategies when practically implemented into a real solar plant, taking into account realistic plant parameters and real meteorological data over a full-year operation. Several important conclusions can be drawn:

- If the superiority of hybrid *compact* power plants over conventional CSP plants was left unclear, the present model

tends to confirm that this family of hybrid approaches systematically demonstrates higher energy output than their pure solar thermal counterparts (the gap between *compact* hybrid and conventional CSP plants tending to grow substantially with increasing PV efficiency).

- Both hybrid strategies show a disproportionate share between the energy output of PV and CSP subsystems. Improving the ability of PV cells to approach their own theoretical limit, through R&D efforts, will impact the system performance in different ways: an improvement in the PV efficiency of the *1S* system will lead to a net gain in the energy output of the plant, without improving the balance with the CSP subsystem. On the other hand, *HT* systems will benefit from an improvement in cell technology, both in terms of energy output and balance between PV/CSP.

- The comparison of hybrid systems encompassing two widely used PV cell materials and characterized by rather different bandgaps (1.4 eV in the case of GaAs, 2 eV in the case of AlGaInP) suggests that tailoring the electronic gap of the cell to ensure a relatively satisfying balance between PV and CSP may lead to a lower energy output: this implies that the optimal opto-electronic properties of the PV cells used in both approaches should stem from a compromise between net energy output of the system and balance between PV and CSP, a point left for future investigations.

- The benefit in the energy output associated with *compact*-hybrid systems tends to reduce as the operating temperature of the CSP converter increases. There is currently a significant body of research dedicated to the development of high-temperature CSP plants , that could translate into higher CSP efficiency in the near future, thus lowering even more the energy gap one may observe between *compact*-hybrid and conventional CSP plants. In the meantime, the lifetime of PV cells exposed to increasing operating temperature is known do decrease significantly, and the development of efficient and reliable *HT* modules operating at temperatures of hundreds of degrees will necessarily require this reliability issue to be successfully addressed.

Several additional remarks are in order:
As already stated previously, there is a large gap in the technological maturity of the two types of PV converters considered in this work. Flat-panel single-junction GaAs solar cells are already produced at an industrial scale and show very high efficiency, both at the cell and module level. This cell technology will thus require minor research efforts before its integration into *1S compact*-hybrid power plants, that will mainly consist in ensuring the most efficient spectrum-splitting possible. Conversely, the development of efficient *HT* solar cells is currently highly speculative, despite promising first attempts . Major progress will need to be achieved, both at the cell and module level, before considering their integration into *HT compact*-hybrid power plants.

Acknowledgment

The authors would like to acknowledge the financial support from the "Région Occitanie" (decision 2018001074/Aldoct-000478) as well as the French "Investments for the future" ("Investissements d'Avenir") programme managed by the National Agency for Research (ANR) under contract ANR-10-LABX-22-01 (labex SOLSTICE).

References

[1] A. Jäger-Waldau, Snapshot of photovoltaics—february 2019, Energies 12 (5) (2019) 769.
[2] X. Ju, C. Xu, Y. Hu, X. Han, G. Wei, X. Du, A review on the development of photovoltaic/concentrated solar power (pv-csp) hybrid systems, Solar Energy Materials and Solar Cells 161 (2017) 305–327.
[3] K. Larchet, Solar pv-csp hybridisation for baseload generation: A techno-economic analysis for the chilean market (2015).
[4] H. Liu, R. Zhai, J. Fu, Y. Wang, Y. Yang, Optimization study of thermal-storage pv-csp integrated system based on ga-pso algorithm, Solar energy 184 (2019) 391–409.
[5] X. Han, C. Xu, X. Ju, X. Du, Y. Yang, Energy analysis of a hybrid solar concentrating photovoltaic/concentrating solar power (cpv/csp) system, Science Bulletin 60 (4) (2015) 460–469.
[6] X. Han, G. Zhao, C. Xu, X. Ju, X. Du, Y. Yang, Parametric analysis of a hybrid solar concentrating photovoltaic/concentrating solar power (cpv/csp) system, Applied energy 189 (2017) 520–533.
[7] T. P. Otanicar, R. Wingert, M. Orosz, C. McPheeters, Concentrating photovoltaic retrofit for existing parabolic trough solar collectors: Design, experiments, and levelized cost of electricity, Applied Energy 265 (2020) 114751.
[8] W. Qu, X. Xing, Y. Cao, T. Liu, H. Hong, H. Jin, A concentrating solar power system integrated photovoltaic and mid-temperature solar thermochemical processes, Applied Energy 262 (2020) 114421.
[9] F. Dominio, Techno-economic analysis of hybrid pv-csp power plants. advantages and disadvantages of intermediate and peak load operation, Master's thesis, Universitat Politècnica de Catalunya (2014).
[10] L. Bousselamti, M. Cherkaoui, Modelling and assessing the performance of hybrid pv-csp plants in morocco: A parametric study, International Journal of Photoenergy (2019).
[11] C. Valenzuela, C. Mata-Torres, J. M. Cardemil, R. A. Escobar, Csp+ pv hybrid solar plants for power and water cogeneration in northern chile, Solar Energy 157 (2017) 713–726.
[12] X. Ju, C. Xu, Z. Liao, X. Du, G. Wei, Z. Wang, Y. Yang, A review of concentrated photovoltaic-thermal (cpvt) hybrid solar systems with waste heat recovery (whr), Science bulletin 62 (20) (2017) 1388–1426.
[13] X. Ju, C. Xu, X. Han, X. Du, G. Wei, Y. Yang, A review of the concentrated photovoltaic/thermal (cpvt) hybrid solar systems based on the spectral beam splitting technology, Applied Energy 187 (2017) 534–563.
[14] B. Widyolar, L. Jiang, J. Ferry, R. Winston, A. Kirk, M. Osowski, D. Cygan, H. Abbasi, Theoretical and experimental performance of a two-stage (50x) hybrid spectrum splitting solar collector tested to 600 °C, Applied energy 239 (2019) 514–525.
[15] B. Widyolar, L. Jiang, J. Ferry, R. Winston, et al., Experimental performance of a two-stage (50x) parabolic trough collector tested to 650 c using a suspended particulate (alumina) htf, Applied Energy 222 (2018) 228–243.
[16] T. Zhu, Q. Li, Y. Xuan, D. Liu, H. Hong, Performance investigation of a hybrid photovoltaics and mid-temperature methanol thermochemistry system, Applied Energy 256 (2019) 113908.
[17] T. Otanicar, J. Dale, M. Orosz, N. Brekke, D. DeJarnette, E. Tunkara, K. Roberts, P. Harikumar, Experimental evaluation of a prototype hybrid cpv/t system utilizing a nanoparticle fluid absorber at elevated temperatures, Applied energy 228 (2018) 1531–1539.
[18] X. Ju, M. M. Abd El-Samie, C. Xu, H. Yu, X. Pan, Y. Yang, A fully coupled numerical simulation of a hybrid concentrated photovoltaic/thermal system that employs a therminol vp-1 based nanofluid as a spectral beam filter, Applied Energy 264 (2020) 114701.

[19] X. Han, X. Chen, Y. Sun, J. Qu, Performance improvement of a pv/t system utilizing ag/coso4-propylene glycol nanofluid optical filter, Energy 192 (2020) 116611.
[20] K. Fisher, Z. Yu, R. Striling, Z. Holman, Pvmirrors: Hybrid pv/csp collectors that enable lower lcoes, in: AIP Conference Proceedings, Vol. 1850, AIP Publishing LLC, 2017, p. 020004.
[21] Z. J. Yu, K. C. Fisher, X. Meng, J. J. Hyatt, R. P. Angel, Z. C. Holman, Gaas/silicon pvmirror tandem photovoltaic mini-module with 29.6% efficiency with respect to the outdoor global irradiance, Progress in Photovoltaics: Research and Applications 27 (5) (2019) 469–475.
[22] J. Y. Zhengshan, K. C. Fisher, B. M. Wheelwright, R. P. Angel, Z. C. Holman, Pvmirror: a new concept for tandem solar cells and hybrid solar converters, IEEE Journal of Photovoltaics 5 (6) (2015) 1791–1799.
[23] L. Huaxu, W. Fuqiang, Z. Dong, C. Ziming, Z. Chuanxin, L. Bo, X. Huijin, Experimental investigation of cost-effective zno nanofluid based spectral splitting cpv/t system, Energy 194 (2020) 116913.
[24] X. Han, C. Xu, X. Pan, X. Ju, X. Du, Dynamic analysis of a concentrating photovoltaic/concentrating solar power (cpv/csp) hybrid system, Science China Technological Sciences 62 (11) (2019) 1987–1998.
[25] J. B. Lasich, I. Thomas, P. J. Verlinden, A. Lewandowski, W. Heartag, M. Wright, Comparative performance assessment for central receiver cpv systems, in: AIP Conference Proceedings, Vol. 1407, American Institute of Physics, 2011, pp. 374–377.
[26] J. Lasich, I. Thomas, W. Hertaeg, D. Shirley, N. Faragher, N. Erenstrom, S. Carter, B. Cox, X. Zuo, A 200kw central receiver cpv system, in: AIP Conference Proceedings, Vol. 1679, AIP Publishing LLC, 2015, p. 030004.
[27] J. Zeitouny, N. Lalau, J. M. Gordon, E. A. Katz, G. Flamant, A. Dollet, A. Vossier, Assessing high-temperature photovoltaic performance for solar hybrid power plants, Solar Energy Materials and Solar Cells 182 (2018) 61–67.
[28] A. Vossier, J. Zeitouny, E. Katz, A. Dollet, G. Flamant, J. Gordon, Performance bounds and perspective for hybrid solar photovoltaic/thermal electricity-generation strategies, Sustainable Energy & Fuels 2 (9) (2018) 2060–2067.
[29] J. M. Gordon, T. Fasquelle, E. Nadal, A. Vossier, Providing large-scale electricity demand with photovoltaics and molten-salt storage, Renewable and Sustainable Energy Reviews 135 (2021) 110261.
[30] A. Baker, A. Skinrood, Characteristics of current solar central receiver projects, Tech. rep., Sandia National Labs., Livermore, CA (USA) (1987).
[31] A. Ferriere, M. Volut, A. Perez, Y. Volut, In-situ measurement of concentrated solar flux and distribution at the aperture of a central solar receiver, in: AIP Conference Proceedings, Vol. 1734, AIP Publishing LLC, 2016, p. 130007.
[32] M. Rodríguez-Sánchez, C. Leray, A. Toutant, A. Ferriere, G. Olalde, Development of a new method to estimate the incident solar flux on central receivers from deteriorated heliostats, Renewable Energy 130 (2019) 182–190.
[33] M. A. Green, E. D. Dunlop, J. Hohl-Ebinger, M. Yoshita, N. Kopidakis, X. Hao, Solar cell efficiency tables (version 56), Progress in Photovoltaics: Research and Applications 28 (7) (2020) 629–638.
[34] E. E. Perl, J. Simon, J. F. Geisz, M. L. Lee, D. J. Friedman, M. A. Steiner, Measurements and modeling of iii-v solar cells at high temperatures up to 400 °C, IEEE Journal of Photovoltaics 6 (5) (2016) 1345–1352.
[35] V. Ganapati, T. P. Xiao, E. Yablonovitch, Ultra-efficient thermophotovoltaics exploiting spectral filtering by the photovoltaic band-edge, arXiv preprint arXiv:1611.03544 (2016).
[36] S. Moreno-Tejera, L. Ramírez-Santigosa, M. Silva-Pérez, A proposed methodology for quick assessment of timestamp and quality control results of solar radiation data, Renewable Energy 78 (2015) 531–537.
[37] M. J. Wagner, T. Wendelin, Solarpilot: A power tower solar field layout and characterization tool, Solar Energy 171 (2018) 185–196.
[38] K.-H. Lee, K. Araki, L. Wang, N. Kojima, Y. Ohshita, M. Yamaguchi, Assessing material qualities and efficiency limits of iii–v on silicon solar cells using external radiative efficiency, Progress in Photovoltaics: Research and Applications 24 (10) (2016) 1310–1318.
[39] J. C. Fan, Theoretical temperature dependence of solar cell parameters, Solar cells 17 (2-3) (1986) 309–315.
[40] S. P. Ayeng'o, H. Axelsen, D. Haberschusz, D. U. Sauer, A model for direct-coupled pv systems with batteries depending on solar radiation, temperature and number of serial connected pv cells, Solar Energy 183 (2019) 120–131.
[41] A. Vossier, F. Gualdi, A. Dollet, R. Ares, V. Aimez, Approaching the Shockley-Queisser limit: General assessment of the main limiting mechanisms in photovoltaic cells, Journal of Applied Physics 117 (1) (2015).
URL https://hal-univ-perp.archives-ouvertes.fr/hal-01176339
[42] T. J. Silverman, M. G. Deceglie, B. Marion, S. Cowley, B. Kayes, S. Kurtz, Outdoor performance of a thin-film gallium-arsenide photovoltaic module, in: 2013 IEEE 39th Photovoltaic Specialists Conference (PVSC), 2013, pp. 0103–0108.
[43] E. Skoplaki, J. A. Palyvos, On the temperature dependence of photovoltaic module electrical performance: A review of efficiency/power correlations, Solar energy 83 (5) (2009) 614–624.
[44] R. Zhai, Y. Chen, H. Liu, H. Wu, Y. Yang, Optimal design method of a hybrid csp-pv plant based on genetic algorithm considering the operation strategy, International Journal of Photoenergy (2018).
[45] E. E. Perl, J. Simon, D. J. Friedman, N. Jain, P. Sharps, C. McPheeters, Y. Sun, M. L. Lee, M. A. Steiner, (al) gainp/gaas tandem solar cells for power conversion at elevated temperature and high concentration, IEEE Journal of Photovoltaics 8 (2) (2018) 640–645.
[46] M. A. Green, E. D. Dunlop, D. H. Levi, J. Hohl-Ebinger, M. Yoshita, A. W. Ho-Baillie, Solar cell efficiency tables (version 54), Progress in photovoltaics: research and applications 27 (7) (2019) 565–575.
[47] Champion photovoltaic module efficiency chart, https://www.nrel.gov/pv/module-efficiency.html (2019).
[48] B. Ehrhart, D. Gill, Evaluation of annual efficiencies of high temperature central receiver concentrated solar power plants with thermal energy storage, Energy Procedia 49 (2014) 752–761.
[49] Y. Jannot, Transferts thermiques, Ecole des mines Nancy (2012) 161.
[50] A. internationale pour l'évaluation du rendement scolaire, Technology roadmap solar thermal electricity, OECD Publishing, 2015.
[51] H. M. Branz, W. Regan, K. J. Gerst, J. B. Borak, E. A. Santori, Hybrid solar converters for maximum exergy and inexpensive dispatchable electricity, Energy & Environmental Science 8 (11) (2015) 3083–3091.